PAPER • **OPEN ACCESS**

Estimation of terrain's linear deformation rates using synthetic aperture radar systems

To cite this article: Cosmin Dnior *et al* 2018 *IOP Conf. Ser.: Mater. Sci. Eng.* **400** 022018

Estimation of terrain's linear deformation rates using synthetic aperture radar systems

Cosmin Dănișor[1], Mihai Datcu[1,2], Alin Dănișor[3]
[1]University Politehnica of Bucharest, Faculty of Electronics, Telecommunications and Information Technology 1-3 Iuliu Maniu Avenue, 061071, Bucharest, Romania
[2]Institute of Remote Sensing and Technology German Aerospace Center, Münchener Straße 20, 82234, Wessling, Germany
[3]Constanta Maritime University, Faculty of Naval Electromechanics, 104 Mircea cel Batran Street, 900663 Constanta, Romania

E-mail: alin.danisor@cmu-edu.eu

Abstract. Synthetic Aperture Radars (SAR) are currently one of the most popular systems in the remote sensing domain, being widely utilized in the earth observation field. Their range of applicability extends in both marine and terrestrial regions. In the maritime domain, SAR systems are intensively used for the study of oceanic waves, waves breaking, marine currents, underwater topography, oil stains, for monitoring the glacier's ice flow, and also for ships detection and localization. In the land areas, a class of applications which exploits the coherence propriety of SAR signals is able to retrieve information related to terrain's characteristics, like topography and displacements. In this work, a processing chain for linear deformation rates estimation is presented and implemented on a dataset of 30 SAR images of Buzău and Focșani cities regions (Romania). The algorithm is based on identification of targets with stable electromagnetic response, exploiting their temporal coherence to obtain reliable estimates. An iterative phase regression analysis is conducted exclusively in the set of detected stable targets. The main challenge is represented by the estimation of the residual component of the phase, due to its random nature. Main feature of the proposed processing chain consists in the fact that it includes a step for terrain's topography estimation, instead of using an external digital elevation model.

1. Introduction

Synthetic Aperture Radar (SAR) systems [1] represent an extension of classical radars. They consist in an antenna mounted on an airborne or space-borne platform which moves with a constant velocity relative to the illuminated scene. Flight direction of the sensor is called azimuth, while the antenna – target direction, perpendicular on the flight path is named range. The system emits coherent pulses in the scene's way and stores the received echoes. Those echoes are then focused using two independent matched filters [1], and a complex image of the illuminated area is formed. This allows the localization of the targets in the range-azimuth plane. Amplitude of each pixel from the images is proportional with the backscattered radiation quantity, while its phase is directly dependent on the sensor – scene distance. Range resolution of those imaging systems is inverse proportional with the emitted pulses bandwidth. To obtain a fine compromise between a low pulse duration and a sufficient quantity of transmitted energy, the pulses are frequency modulated. Their instant frequency presents a

linear variation, therefore chirp signal pulses are emitted. In azimuth direction, the relative velocity between sensor and scene, which leads to an extended illumination time for each target, is exploited. As a consequence, pulses reflected by the same target will present different Doppler frequencies, which allows the synthetization of a larger aperture antenna, which in turn leads to an improvement of azimuth resolution [1]. Therefore, main advantages of SAR systems over classical radars consist in the ability of 2D targets localization, and the possibility to improve the azimuth resolution without extending the physical dimensions of the antenna.

Some benefits of SAR relative to optical surveillance systems can also be outlined. SAR are active illuminating systems, using their own radiation, and as a consequence can operate independently of sunlight: the acquisition of images is possible also during night time. They operate in microwaves domain, which offers cloud penetrating capability, and implicitly the ability to operate independently of weather conditions. The fact that they are coherent systems allows the possibility to extract additional information from the phase of the focused complex images. They use polarized radiation, thus polarization signatures of the targets can be exploited to obtain further details related to the scattering structure [2].

A wide range of processing techniques, which capitalize on the mentioned advantages of those systems has been developed to extract the information available in the focused SAR images. SAR interferometry [3] is based on the coherence propriety of the signals, combining the phase of at least two complex images of the same scene, acquired from different sensor positions. The distance between sensors' positions from which the scene is illuminated is represented by the perpendicular baseline. As the phase is dependent on the sensor-target distance, this method allows the measurement of path related differences with millimetre accuracy. SAR polarimetry [2] is based on the construction of full targets' scattering matrix, which offers information related to their orientation and dielectric proprieties. Exploitation of polarimetric characteristics for both natural and man-made scatterers allows the extraction of quantitative and qualitative information related to their physical characteristics. SAR tomography [4] represents an extension of the processing techniques into the 3D space, by inclusion of a supplementary dimension, perpendicular to the range-azimuth plane of the focused SAR images: the elevation direction. It exploits the baselines diversity of a multiple acquisitions dataset, to estimate the scene's reflectivity profile in elevation direction. This allows the possibility to separate the contributions of scatterers interfering within the same resolution cell. An automatic analysis and interpretation of data can be derived from SAR images segmentation [6], which separates the regions in which radar's reflectivity is constant. Information theory related processing algorithms can be applied for SAR images classification [5], which marks each pixel as belonging to one general group.

SAR are very useful systems in the field of maritime engineering [6], especially for the study of oceanic surface. This represents a complex process, but has high potential because of the diversified number of features that can be extracted. SAR are widely used for sea ice study and monitoring, a practical process for navigation and global climate characterization. Sea ice is probably the most complex earth's surface, its dynamic being continuously influenced by ocean and atmosphere. Due to their mentioned proprieties, SAR instruments represent the most popular choice for study of polar regions, which are frequently covered by clouds and where dark settles for 6 months a year. SAR systems are also ideal for waves study [6], due to the ability to acquire high resolution images of the oceans in all weather conditions. Furthermore, if waves height is below a limit, statistical analysis of the waves proprieties can be computed using linear processing mechanisms, starting from SAR images spectrum. This allows the facile development of waves modelling and prediction algorithms. Those methods have a direct impact in ships design and in the navigation systems, being required because waves have multiple interactions with atmosphere, oceanic currents and underwater topography. Near shore water regions present an interesting case study because of their dynamics, mainly caused by changeable water depths, which also affects waves behaviour. Main application of SAR systems in those regions represents the study of waves refraction and identification of areas were waves breaking occurs. Ocean currents have a major impact on global and local climate. A great influence is caused by

the events occurring at the boundaries of currents systems. Those areas induce changes in ocean's surface roughness, and can be easily detected in SAR images, acquired even in cloudy regions. Upwelling is a phenomenon which occurs mainly in coastal areas, which usually have intense fishing activity, therefore its monitoring from space is important. Ocean surface signatures corresponding to this phenomenon can be detected by the SAR systems. Underwater topography study is essential for activities like shipping, cables laying, or detection of coastal regions prone to hazards [6]. In certain conditions, SAR systems can detect features of underwater topography, and this can reduce the number of expensive naval surveillances. Oil stains from oceans and seas surface are visible in SAR images. This allows their localization, monitoring their dimensions, identification of their sources (ships operations, oil platforms, industrial plants, etc.), and verification of standards compliance in case of ship discharges and tank washing. Ships can also be easily identified in SAR images, from direct radiation reflected in radar's direction or from wake patterns. Level of the power backscattered by oceans' surface is dependent on wind's direction and intensity, so SAR systems can be exploited for wind's vector measurements, proving a useful tool for weather forecasting. Mesoscale atmospheric storms, which directly affect sea's surface roughness can also be monitored with SAR tools.

SAR systems are also intensively used for land related applications. Signals coherence propriety allows the estimation of topographic height, which offers the possibility of accurate Digital Elevation Models (DEM) computation. The phase differences between complex SAR images can be exploited to estimate the terrain's displacements [3], therefore offering the potential for monitoring the effects of natural disasters like earthquakes, landslides or volcanic eruptions. Advanced processing techniques [7] conducted on multi-temporal datasets can be employed for estimation of terrain's linear deformation rates, and implicitly for the examination of the land subsidence phenomenon. The study of backscattered signal proprieties can lead to the delimitation of various region types on the land area, like urban regions, forests, agricultural fields, roads. Moreover, time frequency analysis has been applied for ground moving targets indication [8], with direct applicability in traffic monitoring. Polarimetry related characteristics of the signal can be exploited to estimate the soil moisture levels and surfaces' roughness. Those features are useful also in case of studying the natural disasters effects, being applied for monitoring the floods extent, drought effects and forest fires. Vegetation structure estimation is also intensively applied for ecosystem monitoring purposes, through applications like forests heights computation and agricultural land structure derivation. Examination of targets scattering and polarimetry related parameters variation along a temporal series of SAR images form the basics of change detection algorithms, with large applicability in environmental monitoring and military purposes [2]. Reconstruction of scenes' elevation reflectivity profiles in urban areas allows the possibility to estimate the height of buildings, with the prospect to extend the estimation process to also derive the linear deformation rates and thermal dilation of the analysed structures [4].

This paper is structured as follows: section 2 presents the general theoretical aspects of SAR interferometry, section 3 describes the dataset on which the experiment was conducted, while the processing chain is detailed in section 4, along with intermediate and final results preentation. Last section is dedicated to the conclusions.

2. SAR Interferometry: from initial approaches to advanced multi-temporal techniques

As mentioned in previous section, SAR interferometry (InSAR) [3] exploits the coherence propriety of the signals, being able to extract information related to terrain's height, displacements or deformation rates from the phase of SAR images. Interferometric phase represents the phase difference between two focused images of the same region, acquired simultaneously from different sensors positions, or at different moments of time during repeated surveillances of the area. The interferogram is generated by pixel by pixel multiplication of the reference (master) image with the complex conjugate of the slave acquisition. Main components of the interferometric phase Φ_{itf} are:

$$\phi_{itf} = \phi_{fl} + \phi_{topo} + \phi_{def} + \phi_{atm} + \phi_n \quad (1)$$

where Φ_{fl} component represents the contribution of earth's surface curvature, Φ_{topo} is proportional with terrain's altitude, Φ_{disp} quantifies the scene's displacements which occurred in the temporal interval delimited by the moments of the two acquisitions (called temporal baseline, in case of repeat pass interferometry, where the images are acquired during distinct surveillances of the scene), Φ_{atm} is related to the non-uniform propagation of waves through atmosphere, and Φ_n represent the system's noise

By estimating the topography, this technique allows the 3D positioning of the scatterers. Topographic component is also proportional with the perpendicular baseline b_p of the two acquisitions:

$$\phi_{topo} = \frac{4\pi}{\lambda} \frac{b_p}{R \sin\theta} h \tag{2}$$

where λ represents the radar's wavelength, R the distance between sensor and scene, θ the incidence angle (the angle under which the scene is illuminated by the radar, relative to the vertical direction), and h denotes the terrain's height. Therefore, in order to estimate scene's topography, it is mandatory that the images from which interferogram is generated are acquired from different sensor's positions. The sensitivity of interferometric phase to terrain's altitude increases with perpendicular baseline's value. However, this parameter (b_p) introduces a spectral shift to scatterer's response and should be kept below an upper limit, called critical baseline, otherwise the frequency bands of targets' spectral responses from the two images will not overlap, preventing the extraction of common information. To prevent the influence of the temporal decorrelation, the images should present a short temporal baseline. Ideally, they should be simultaneously acquired. Usually, when this desiderate is not possible, images are obtained during consecutive surveillances of the interest area.

Differential interferometry [3] analyses the deformation patterns of the scene. Displacements component Φ_{disp} of the interferometric phase is directly influenced by the variations of terrain's height δr which occurred between the acquisition moments of the interferometric images pair:

$$\phi_{def} = \frac{4\pi}{\lambda} \delta r \tag{3}$$

Differential interferometry (D-InSAR) separates the above component from the interferometric phase in order to retrieve scene's displacements. To achieve this objective, earth's curvature contribution term Φ_{fl} can be estimated from informations related to satellite's orbit trajectories from the images acquisition process. The topographic component can be estimated from an external DEM: the case of 2-pass D-InSAR. This method requires the conversion of DEM to the acquisition geometry of the images, from ground geometry to SAR geometry. Other approaches of differential interferometry estimate the DEM from a pair of complex SAR acquisitions (called topographic pair). The estimated heights are used to subtract the topographic component from the interferometric phase which also contains the displacements effects (differential pair). The topographic and differential image pairs can have a common reference image, in which case a total of 3 acquisitions of the scene are required (3-Pass D-InSAR). Topographic and differential pairs can also contain distinct images (4-Pass D-InSAR). D-InSAR technique is popular for estimation of natural disasters' consequences. If 3 or 4-pass methods are employed, images that form the topographic pair should both be acquired before natural disaster's appearance and, ideally, should have long perpendicular and short temporal baselines. The interval between the acquisitions of differential images pair should contain the moment of natural disaster's occurrence and, ideally, should present a short perpendicular baseline, to limit the temporal decorrelation.

Residual component of interferometric phase, which contains the effects of non-uniform signals propagation through atmosphere (caused mainly by the variable vapour content of troposphere), temporal decorrelation and system noise, is difficult to estimate due to its stochastic nature. This led to the development of advanced differential interferometry techniques (A-D-InSAR) [7], which utilize multiple acquisitions of the same scene. Those multi-temporal methods study the variation of

interferometric phase during a large temporal interval, across multiple interferograms, to estimate the residual interferometric term. This phase regression analysis also allows the evaluation of area's linear deformation rates. One of the most popular A-D-InSAR methods is based on identification of targets candidates from which the information can be successfully extracted. Those points, called Persistent Scatterers (PS), present stable electromagnetic proprieties over time, and are suitable for analysis since their temporal decorrelation is low. Persistent Scatterers Interferometry (PS-InSAR) [9] conducts the phase regression analysis solely in those stable targets, leading to reliable estimations for residual component and for target's deformation signatures. Small baselines subset (SBAS) algorithm [10] exclusively analyses the differential interferograms generated from image pairs characterized by a low perpendicular baseline, in order to limit the geometrical decorrelation induced by the aforementioned spectral shifts.
In this paper, an interferometric processing chain based on PS-InSAR method is applied on a multi-temporal dataset for estimation of linear deformation rates from two urban regions.

3. SAR images dataset

The multi-temporal dataset consists in 30 complex images if Buzău-Brăila-Focșani region, Romania, acquired by ERS satellite constellation between May 1995 and June 2000. European Remote Sensing (ERS) was the first SAR mission coordinated by European Space Agency (ESA). It consisted of two satellites, ERS-1 (active between 1991 and 2000) and ERS-2 (active between 1995 and 2011). During their common operational time, those satellites formed a tandem mission, the same ground point being illuminated by both satellites within 24 hours. Their orbital repeat cycle was equal to 35 days. The sensors operated in C band, the radar frequency being equal to 5.3 Hz. Ground range resolution of the images is approximately 25 m, while azimuth resolution equals 5 m.

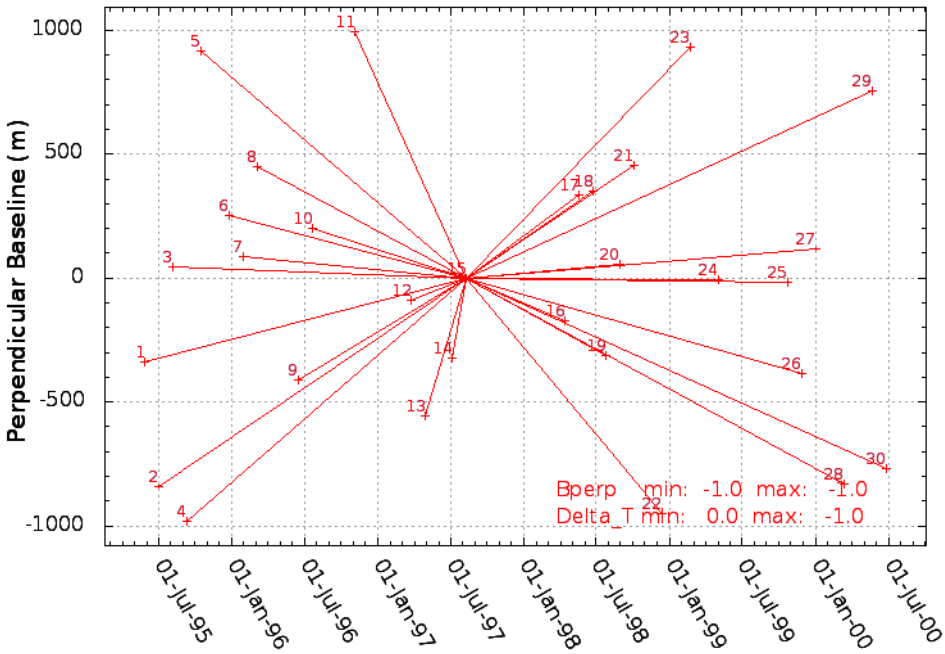

Figure 1. Distribution of acquisition's perpendicular and temporal baselines.

Acquisition date of dataset's master image was chosen near the central point of dataset's temporal span (11.08.1997), to control the temporal decorrelation occurence. Maximization of dataset's perpendicular baseline values dispersion was also considered when choosing the reference image, since this helps reduce the errors of atmospheric phase screen estimation [11]. Dataset presents a perpendicular baselines span of 1974.78 m. Temporal baselines span is equal to 5 years and 1 month. Distribution of dataset's images in spatio-temporal plane is presented in figure 1, where each image is positioned relative to its acquisition date and perpendicular baseline value.

Two test regions in which linear deformation rates estimation process will be implemented were defined. Both images sections contain urban areas, which are regions of interest for subsidence phenomenon study and also present a high probability for stable targets detection. Buzău and Focșani areas were chosen for analysis. Image of Buzău region contains 700 range samples and 1300 azimuth lines (910000 complex pixels), while the image of Focșani area is made of 600 range samples and 1400 azimuth lines (840000 complex pixels). Amplitudes of the two test regions are presented in figure 2.

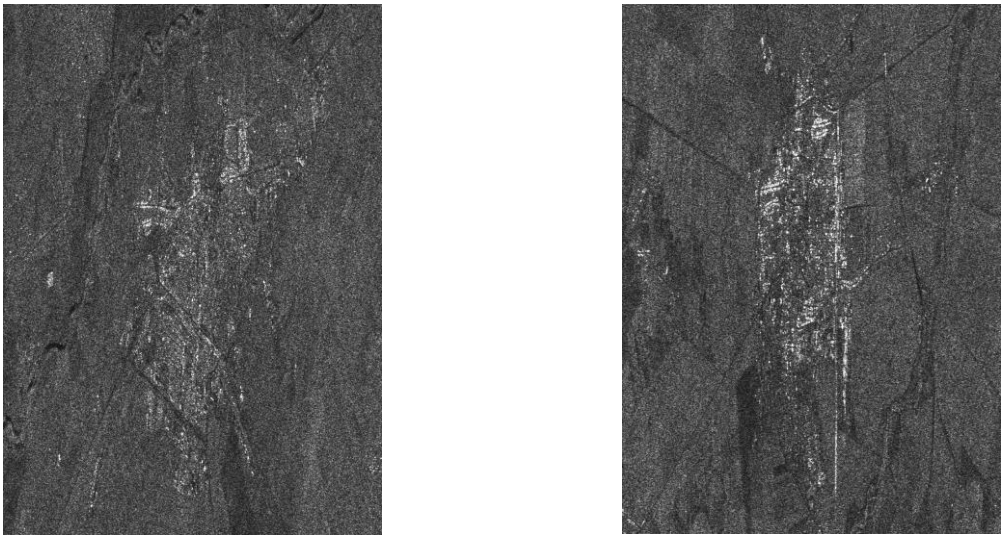

Figure 2. Amplitudes of Buzău (left) and Focșani (right) areas, from master image of the dataset. Acquisition date: 11.08.1997.

Urban regions can be easily distinguished in both images. Due to absence of dispersion phenomenon characteristic to vegetation areas, power of the signal backscattered from stable structures is higher, hence the urban areas appear brighter in the focused SAR images.

4. Linear deformation rates estimation

4.1. Processing chain overview

The processing chain outlined and implemented in this work in order to reach the stated objective is based on PS-InSAR technique. Main processing steps are synthesized in figure 3 and will be detailed in the forthcoming sections:

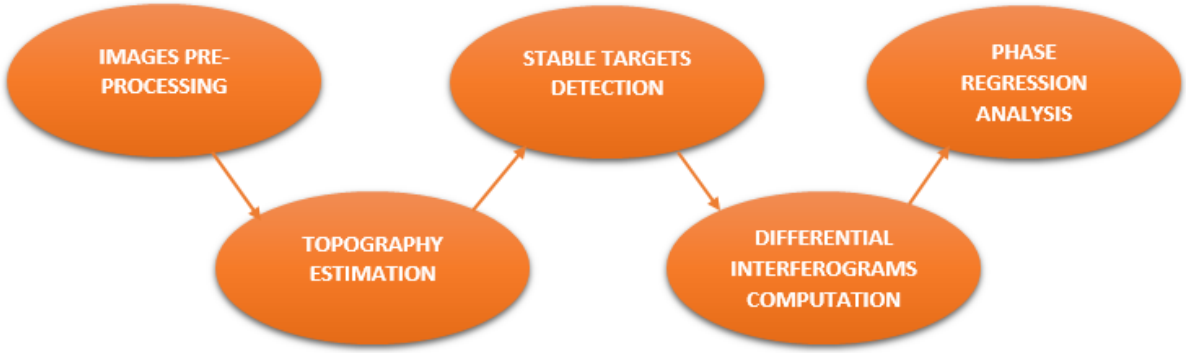

Figure 3. Main steps of the processing chain employed for linear deformation rates estimation.

Main feature of this proposed chain consists in the fact that it includes a step dedicated to the digital elevation model computation. Most published domain-related works [12],[13] prefer the use of an external DEM for estimation of interferometric phase's topographic component. However, computation of the DEM from a suitable couple of dataset's images presents the advantage that the elevation model is directly generated in the acquisition geometry of the reference image and at the same resolution, therefore avoiding the necessity of its conversion from ground to SAR geometry. Also, the resolution of available DEM is usually lower than the one of SAR images, the most popular free DEM source being the SRTM database, whose resolution is between 30 and 90 m. Identification of the areas covered by the SAR images in the external DEM, for perfect alignment also represents a delicate process. Main reason for which generation of terrain's topography from SAR images is usually avoided is given by the fact that topographic component, which is dominant in the intererogram from which the DEM is computed, generates high variations to the interferometric phase, and this aspect can hamper the subsequent steps of the processing.
Subsequent subsections present the theoretical description of the processing chain's steps, along with the results obtained on the two case studies – Buzău and Focșani regions. The algorithm was implemented using the Interferometric SAR Processing and Interferometric Point Targets Analysis packages of the Gamma RS software [14],[15].

4.2. Images pre-processing
Main aim of pre-processing step consists in the compensation of different acquisitions geometries of the images, since the terrain is illuminated from a different position during each surveillance of the sensors (hence the existence of perpendicular baselines). This alignment step of the images, called coregistration, consists in the resampling of slave images in order to overlap the reference image of the dataset. Raw coregistration can be implemented based on satellites orbit trajectories. However, in case of ERS constellation, orbit related information is not accurate, so this step will not be considered. Shifts between an interferometric pair of images will be identified in both range and azimuth directions by maximization of images amplitude cross-correlation R:

$$R = \frac{\sum_{l \in w} A_{ml} A_{sl}}{\sqrt{\sum_{l \in w} A_{ml}^2 \sum_{l \in w} A_{sl}^2}} \tag{4}$$

where A_{ml} and A_{sl} denote the amplitudes of master and slave images, in l^{th} point of w window used for correlation estimation, this parameter being computed in sliding windows, defined across all regions of the images. Maximization of (4) leads to identification of variable offsets in both range and azimuth directions, which form the basis for construction of polynomials that will be employed for slave images' resampling process. For better accuracy, coregistration is usually implemented at sub-pixel level, after oversampling of the images is conducted in spectral domain.
For cross correlation estimation, 128 sliding windows consisting of 32 range samples and 32 azimuth lines were utilized. The over-sampling factor of the images was chosen equal to 4, and hexic polynomials were used for the resampling step. For validation of corregistration process, amplitude's correlation index between the pair of images which will be later used for DEM computation was estimated and analysed. Spatial distributions of this parameter, in both test regions, computed for the images acquired on 07.07 and 11.08.1997, are presented in figure 4:

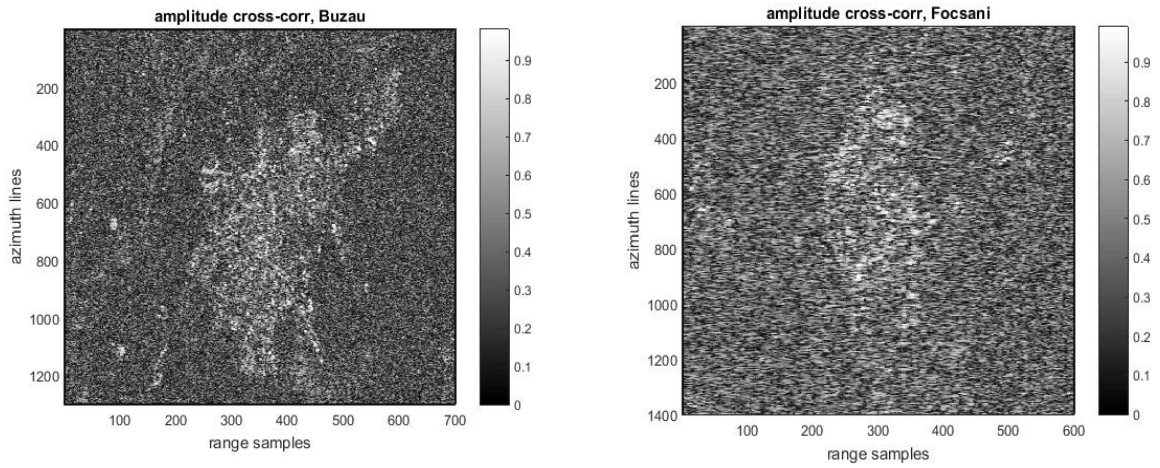

Figure 4. Amplitude's correlation index spatial distribution, interferometric pair 07.07-11.08.1997 Buzău (left) and Focșani (right) regions.

As expected, correlation index values are higher in urban regions, reaching peaks equal to 0.99 in case of both test scenes. Mean value of amplitude's cross-correlation is equal to 0.33 in case of Buzău region and 0.4 in case of Focșani area, acceptable considering that vegetation is present in a large proportion of test scenes. Peak values of cross-correlation are close to the upper limit, which indicates a precise images coregistration process.

4.3. Topography estimation

The pair of images from which the scene's DEM will be estimated was selected in order to ensure that the topographic component will be dominant in the interferometric phase. A couple of acquisitions with minimal temporal baseline of 35 days were selected to reduce the effects of temporal decorrelation. Furthermore, both acquisition were made in the summer period (03.07 – master, 07.08.1995 - slave), to ensure that the terrain was not covered by snow. Perpendicular baseline has a high value, 954.88 m, which helps increase the sensitivity of topographic component to terrain's height.

Main steps of the interferometric processing chain employed for DEM estimation are presented in the diagram from figure 5, and will be detailed below:

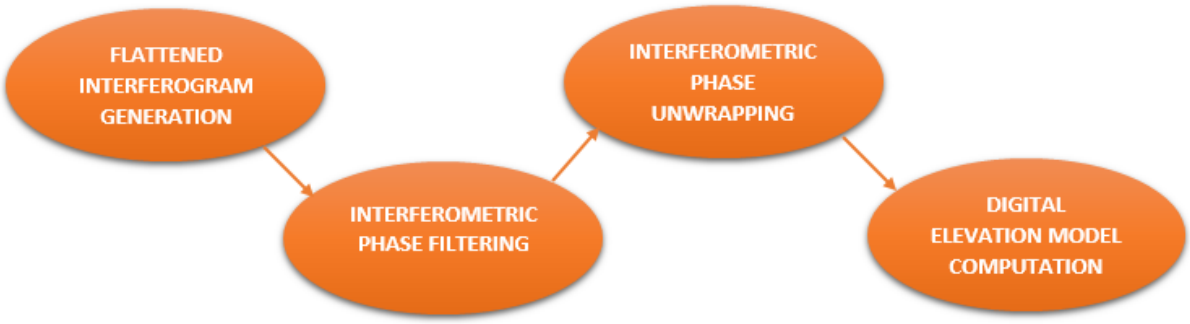

Figure 5. Interferometric processing chain for topography's estimation

The interferogram was generated by pixel by pixel multiplication of master acquisition with slave's complex conjugate. Interferometric phase variation presented in figure 6 contains the components mentioned in equation (1).

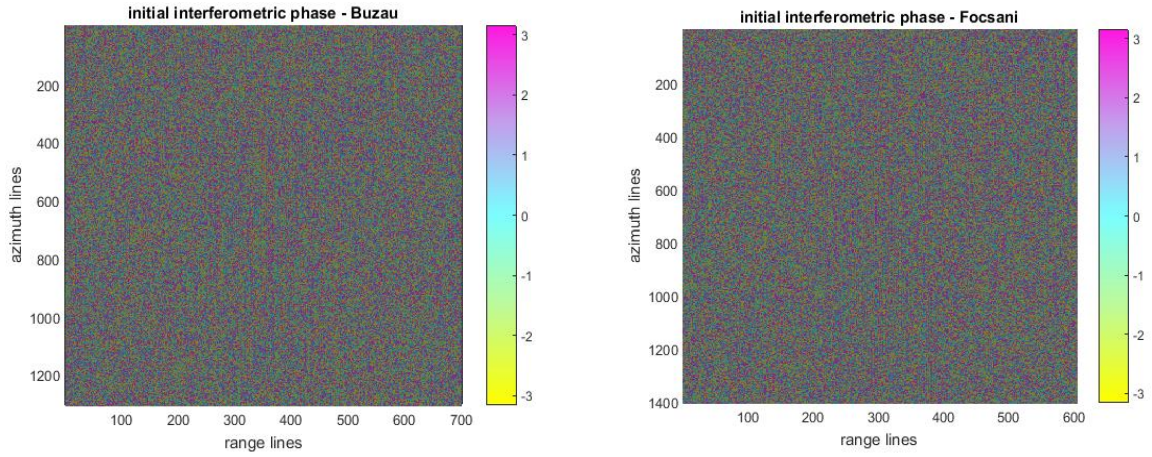

Figure 6. Interferometric phase of topographic images pair (radians), Buzău (left) and Focșani (right) regions.

High density of fringes which is observable the raw interfergoram represents a consequence of earth curvature's surface contribution. This term - Φ_{fl} - is estimated based on orbit state vectors and is subtracted from the interferometric phase, generating the flattened interferograms, whose variations are shown in figure 7:

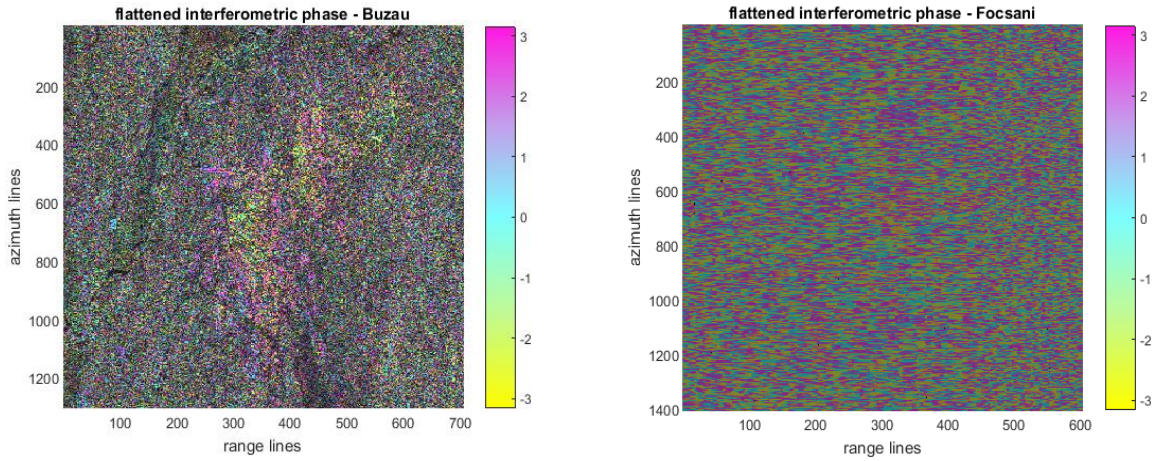

Figure 7. Flattened interferometric phase of the topographic pair (radians), Buzău (left) and Focșani (right) regions.

Interferometric phase filtering is an important process, the results of the further stages of the processing chain being highly dependable on the quality of the filtered phase. To ensure a successful implementation of this step, an adaptive filtering algorithm operating in spectral domain – Goldstein-Werner method [16] – has been utilized. This filter is projected to optimize the visibility of interferometric phase's fringes, having the transfer function *H(i,j)* defined in respect with interferometric power spectrum *I(i,j)*:

$$H(i,j) = I(i,j)^{a} \tag{5}$$

where *a* is a subunit coefficient, whose value represents a compromise between noise suppression degree and interferogram's features conservation. To obtain an equitable trade-off, this parameter was chosen equal to 0.5. The variation of filtered interferometric phase is represented in figure 8:

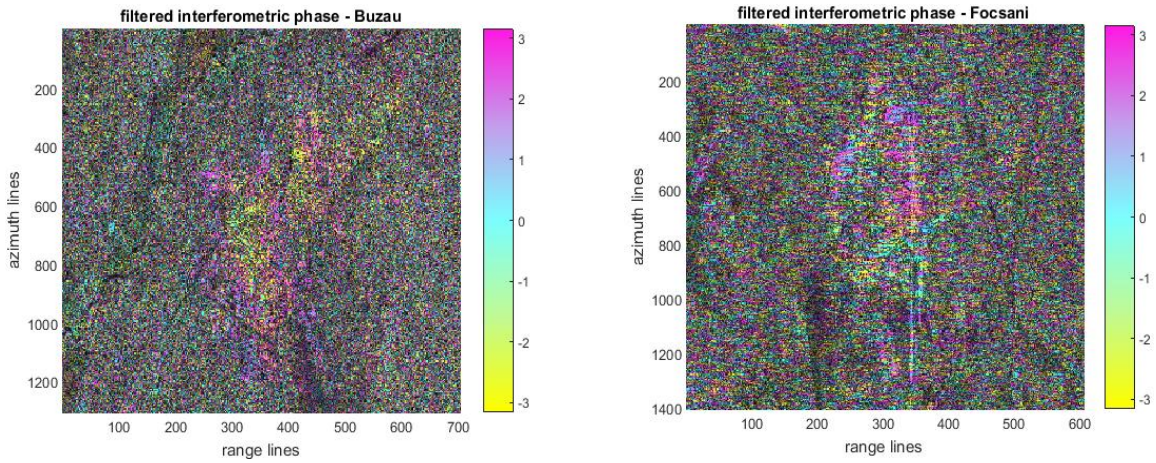

Figure 8. Filtered interferometric phase (radians), Buzău (left) and Focșani (right) regions.

Due to the periodical nature of the signals utilized within the SAR systems, the values of the initial interferometric phase belong to *[0,2π]* interval. A consequence of this fact is the existence of fringes, noticeable in all interefrograms from figures 6-8. Each fringe basically represents a complete phase variation within the *[0,2π]* interval. To be able to extract information from the interferograms, 'real' phase values must be retrieved, by determination of the correct number n of 2π integers which must added to the initial phase values ψ in order to eliminate the ambiguities, this process being called phase unwrapping:

$$\varphi(i,j) = \psi(i,j) + 2\pi n(i,j) \tag{6}$$

Basically, unwrapped interferometric phase φ must be estimated from its modulo 2π values ψ. Main challenge of the unwrapping process is given by the presence of phase discontinuities: loops in which the following propriety is not met:

$$\nabla \times (\nabla \psi) = 0 \tag{7}$$

Basically, the curl of the gradient along the respective loop is not null. Those areas present residues, their main cause being the existance of noise. This confirms the importance of phase filtering step, whose main objective is to reduce the number of residues.
Phase unwrapping was implemented using the minimum network cost flow (MCF) algorithm [17].

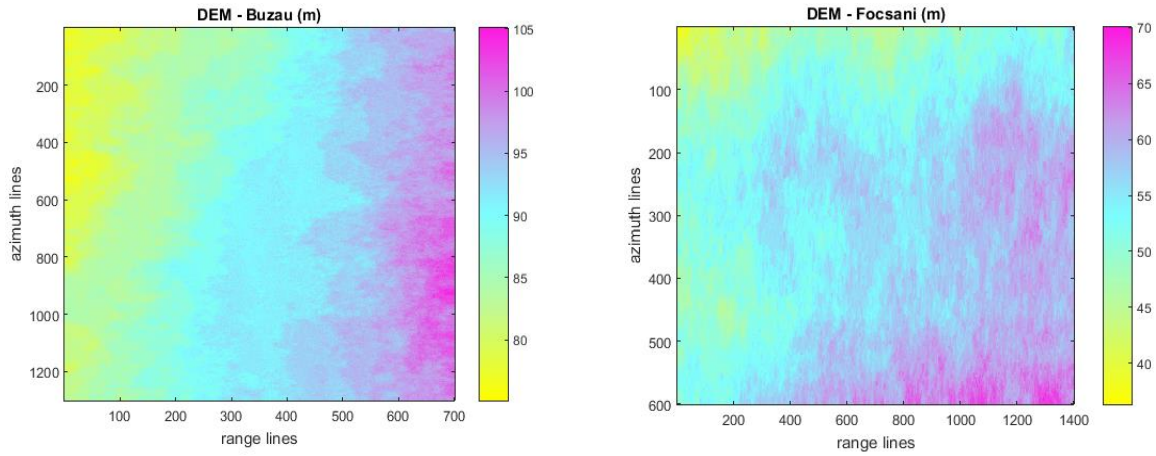

Figure 9. Estimated topography (m), Buzău (left) and Focșani (right) regions.

This method formulates the determination of unknown parameter *n* as a minimization problem with constraints. The restrictions are given by the residues existence, which should be avoided in the unwrapped interferometric phase.
The terrain heights can be derived directly from the unwrapped interferometric phase values, using equation (2). The estimated DEM of Buzău and Focșani regions are presented in figure 9:
In Buzău region, values of the estimated digital terrain model vary between 73 and 105 m, while DEM values of Focșani area belong to 36 and 71 m domain. In both cases, estimated altitudes are close the ones indicated by Google Earth.

4.4. Persistent scatterers detection
Identification of coherent targets, in which the phase regression analysis will be lately conducted, is based on two data analysis: one in temporal and one in spectral domain. Since those coherent points are expected to present a stable response across the SAR images time series, statistics of amplitude's temporal variation will be computed in each resolution cell of the scene. Those statistics are quantified by amplitude's mean per sigma ratio (MSR), which is also directly related to the index of dispersion parameter:

$$A_{MSR} = \frac{\frac{1}{N}\sum_{i=1}^{N} A_i}{\sqrt{\frac{1}{N}\sum_{i=1}^{N}\left(A_i - \frac{1}{N}\sum_{i=1}^{N} A_i\right)^2}} \tag{8}$$

where N is the number of dataset's images, and A_i is the amplitude of the pixel in the i^{th} dataset image. The A_{MSR} index is calculated in each point of the scene. Stable scatterers are characterized by low dispersion of the amplitude, so a target is classified as stable if MSR index is over unity.
Second analysis studies the variation of the spectral coherence's phase, since persistent scatterers are expected to present a stable spectral phase. Power spectral density $q_X(\omega)$ is calculated according to Wiener-Hincin theorem, as the spectrum of data vector's G autocorrelation R_G:

$$q_G(\omega) = \sum_k R_G(k) e^{-j\omega k} \tag{9}$$

Final set of detected persistent scatterers represents the reunion of the subsets identified by the temporal and the spectral analysis. The spatial distributions of the candidates from Buzău and Focșani regions are presented in figure 10:

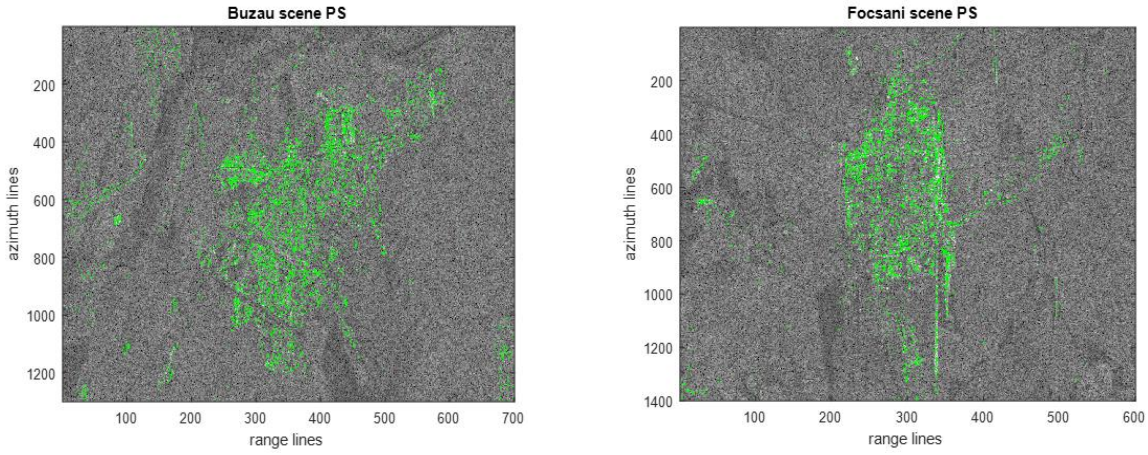

Figure 10. Spatial distribution of detected Persistent Scatterers (green), Buzău (left) and Focșani (right) regions.

A number of 33295 stable scatterers have been detected in Buzău region, and 21462 in Focșani region, which represents 3.65%, respectively 2.55% of test areas total number of resolution cells. As expected, the majority of stable targets have been detected in brighter, urban regions.

4.5. Differential interferograms computation

Flattened interferograms are calculated in the detected stable points from dataset's reference acquisition and each slave image. Therefore, 29 interferograms are generated for each test scene, in the points highlighted in figure 10. To compute the differential interferograms, on which the phase regression analysis will be conducted, topographic component is subtracted from the flattened phase of each interferometric pair. This operation is based on the previously estimated DEM heights, the topographic phase component being calculated individually for each interferogram, as it depends on the perpendicular baseline of the associated image pair, as stated by equation (2).

Phase unwrapping of the differential interferograms is optional, since the regression analysis can also be conducted on the modulo 2π values. Phase of the differential interferograms contains the displacements component and the residual term. Its aspect is also influenced by the perpendicular baseline of the interferometric pair from which it was generated, presenting a more pronounced spatial variation as the perpendicular baseline increases.

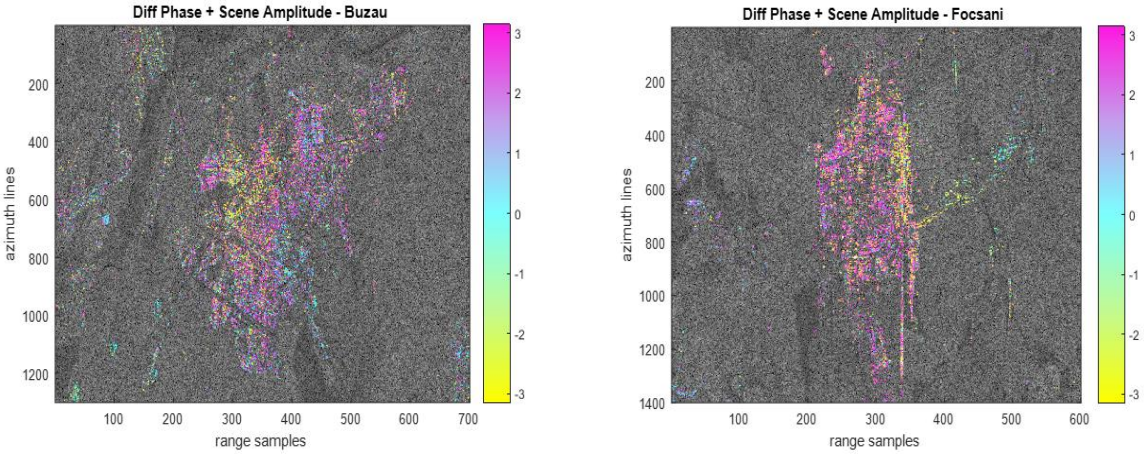

Figure 11. Differential interferometric phase (radians), acquisition pair: 11.08.1997 – 22.06.1998, Buzău (left) and Focșani (right) regions.

Differential interferograms computed in the coherent points of both test regions from the images pair acquired on 11.08.1997 and 22.06.1998 are presented in figure 11. Perpendicular baseline of this interferometric pair equals 355.43 m, being relatively low compared to dataset baseline's span. Therefore, those inteferograms present moderate spatial variations.

4.6. Phase regression analysis

In order to estimate and separate the deformation and residual components from the differential interferograms, a phase regression analysis is conducted. Temporal variation of differential interferometric phase is studied for each detected stable target. Regression analysis takes into account the facts that the subtracted topographic component is proportional with the perpendicular baselines of inteferometric image pairs, and the linear deformation rates term of the phase is, in each interferogram, proportional with the associated temporal baseline.

The regression analysis searches for a best fit solution for the interferometric phase terms, taking also into account potential DEM estimation errors. This is an iterative process, consisting in a two-steps evaluation. First iteration concentrates mainly on identification of estimated topography related errors, which are corrected and a new set of differential interferograms is generated. Main objective of second step consists in the estimation of the residual component of the interferometric phase, respectively the

atmospheric phase screen (APS) and system noise terms. APS represents the large-scale term of the residual phase, and is estimated by means of spatial filtering. Temporal filtering is employed for the noise term estimation.

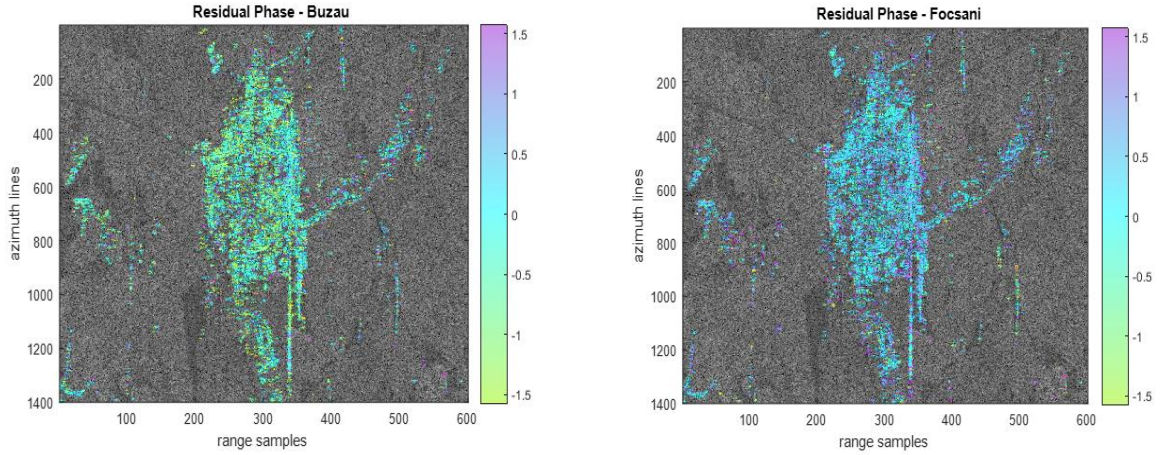

Figure 12. Estimated residual component of the interferometric phase, acquisition pair: 11.08.1997 – 22.06.1998, Buzău (left) and Focșani (right) regions.

Variation of residual interferometric component, estimated for the acquisition pair whose differential interferograms are exemplified in figure 11 (11.08.1997 - 22.06.1998), is represented in figure 12. Since the atmospheric propagation related component, estimated by two-dimensional averaging in range and azimuth directions, is dominant, residual component presents a low spatial variation.

4.7. Results

Once estimated, the residual component is subtracted from the interferometric phase. Variation of the remaining component is proportional with the temporal baselines of the acquisitions, thus allowing the estimation of the linear deformation rates.

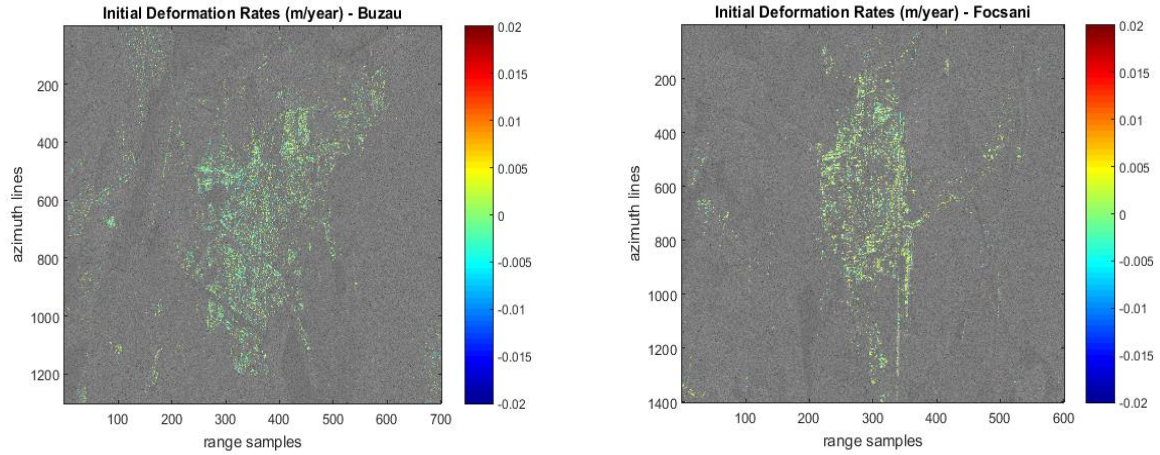

Figure 13. Estimated linear deformation rates (m/year), Buzău (left) and Focșani (right) regions

Estimated linear deformation rates of both test scenes are presented in figure 13. The range of those rates is similar in case of both Buzău and Focșani regions, belonging to -1.5 and 1.5 cm/year domain. In the current stage it is difficult to conduct the validation of the results, the only way to achieve this objective being the comparison with other displacements' measurements conducted in the same area and in the same temporal interval, which are not available. Main cause of this deformation rates is given by the occurrence subsidence phenomenon, in which case the range of the estimated values is realistic.

5. Conclusions

In this paper, a processing chain based on Persistent Scatterers Interferometry was outlined, described and successfully implemented for estimation of linear deformation rates which occurred in the second half of 1990s in the regions of Buzău and Focșani cities. The approached method studies the temporal variation of the phase of the targets with stable electromagnetic proprieties, exploiting their temporal coherence to obtain reliable results. PS detection was conducted based on both temporal and spectral analysis of targets statistics. Compared to similar published works, main feature of the proposed processing chain consists in the fact that it includes a step for terrain's topography estimation, instead of using an external digital elevation model. This route was preferred since the DEM is generated directly in the SAR system's acquisition geometry, with a spatial resolution equal to the one of dataset's images. The most challenging aspect of the implemented processing chain proved to be the estimation of the residual component from the interferometric phase, since its main sources, waves propagation through atmosphere and system noise, can be modelled as stochastic processes. For a better accuracy of the estimation process, an iterative phase regression analysis has been conducted.
Main source of the linear deformation rates is represented by terrain's subsidence. In case of both test regions, absolute estimated values are below 1.5 cm/year. For future work, the experiment will be conducted for the same two regions using a dataset of images acquired by Sentinel 1 mission, which debuted in April 2014, being also operated by European Space Agency. Therefore, a set of linear deformation rates from a different temporal interval will be estimated in both Buzău and Focșani areas, and the results will be compared to the ones presented in this work, for validation of both experiments.

Acknowledgements
This work has been conducted within the frame of research project *SPERO – Space technologies used in the management of disasters and major crises, manifested at local, national and regional levels*, funded from the Minister of Research and Innovation, UEFISCDI, project reference: PN-III-P2-2.1-SOL-2016-03-0046

6. References

[1] Richard B 2000 *Principles of synthetic aperture radar* Surveys in Geophysics **21**(2) pp 147-157
[2] Migliaccio M, Gambardella A and Tranfaglia M 2007 SAR polarimetry to observe oil spills. *IEEE Transactions on Geoscience and Remote Sensing* **45**(2) pp 506-511
[3] Rosen P, Hensley S, Joughin I, Li F, Madsen S, Rodriguez E and Goldstein R 2000 Synthetic aperture radar interferometry *Proceedings of the IEEE* **88**(3) pp 333 - 382
[4] Fornaro O, Serafino F and Soldovieri F 2003 Three-dimensional focusing with multipass SAR data *IEEE Transactions on Geoscience and Remote Sensing* **41**(3) pp 507 - 517
[5] Ferro-Famil L, Pottier E and Lee J S 2001 Unsupervised classification of multifrequency and fully polarimetric SAR images based on the H/A/Alpha-Wishart classifier *IEEE Transactions on Geoscience and Remote Sensing* **39**(11) pp 2332-2342
[6] Jackson C R and John R A 2004 *Synthetic aperture radar: marine user's manual* US Department of Commerce, National Oceanic and Atmospheric Administration, National Environmental Satellite, Data, and Information Serve, Office of Research and Applications
[7] Ferretti A, Fumagalli A, Novali F, Prati C, Rocca F and Rucci A 2011 A New Algorithm for Processing Interferometric Data-Stacks: Squee SAR *IEEE Transactions on Geoscience and Remote Sensing* **49**(9) pp 3460 - 3470
[8] Pettersson M I 2006 Relative speed step size in SAR processing for moving target detection *In Radar, CIE'06. International Conference on* pp 1-5
[9] Ferretti A, Prati C and Rocca F 2001 Permanent scatterers in SAR interferometry *IEEE Transactions on Geoscience and Remote Sensing* **39**(1) 8 - 20
[10] Berardino P, Fornaro G, Lanari R and Sansosti E 2002 A new algorithm for surface deformation monitoring based on small baseline differential SAR interferograms *IEEE Transactions on Geoscience and Remote Sensing* **40**(11) 2375 - 2383

[11] Rocca F 2004 Diameters of the orbital tubes in long-term interferometric SAR surveys *IEEE Geoscience and Remote Sensing* **1**(3) pp 224-227
[12] Lanari R, Berardino P, Bonano M, Casu F, De Luca C, Elefante S and Pepe A 2015 Sentinel-1 results: SBAS-DInSAR processing chain developments and land subsidence analysis In *Geoscience and Remote Sensing Symposium (IGARSS)* 2836-2839
[13] Mora O, Lanari R, Mallorquí J J, Berardino P and Sansosti E 2002 A new algorithm for monitoring localized deformation phenomena based on small baseline differential SAR interferograms *In Geoscience and Remote Sensing Symposium (IGARSS)* pp 1237-1239
[14] ***Gamma Interferometric SAR Processor, ISP User's Guide, 2014
[15] *** Gamma Interferometric Point Targets Analysis Software, IPTA User's Guide, 2014
[16] Hensley S 2017 An Analytic Expression For The Phase Noise Properties Of The Goldstein-Werner Power Spectral Filter *Geoscience and Remote Sensing Symposium (IGARSS)* pp 3802-3805
[17] Costantini M 1998 A novel phase unwrapping method based on network programming *IEEE Transactions on geoscience and remote sensing* **36**(3) 813-821